Published in final edited form as:
Biochemistry. 2013 January 15; 52(2): 355–364. doi:10.1021/bi301567z.

Potent Mechanism-Based Inactivation Of Cytochrome P450 2B4 By 9-Ethynylphenanthrene: Implications For Allosteric Modulation Of Cytochrome P450 Catalysis[1]

Haoming Zhang[§], **Sean C. Gay**[¶,†], **Manish Shah**[¶], **Maryam Foroozesh**[¥], **Jiawang Liu**[¥], **Yoichi Osawa**[§], **Qinghai Zhang**[⊥], **C. David Stout**[⊥], **James R. Halpert**[¶], and **Paul F. Hollenberg**[§,*]

[§]Department of Pharmacology, The University of Michigan Medical School, Ann Arbor, MI 48109, USA

[¶]Skaggs School of Pharmacy and Pharmaceutical Sciences, University of California San Diego, La Jolla, CA 92093, USA

[¥]Department of Chemistry, Xavier University of Louisiana, New Orleans, LA 70125, USA

[⊥]Department of Molecular Biology, The Scripps Research Institute, La Jolla, CA 92037, USA

Abstract

The mechanism-based inactivation of cytochrome P450 2B4 (CYP2B4) by 9-ethynylphenanthrene (9EP) has been investigated. The partition ratio and k_{inact} are 0.2 and 0.25 min^{-1}, respectively. Intriguingly, the inactivation exhibits sigmoidal kinetics with a Hill coefficient of 2.5 and S_{50} of 4.5 μM indicative of homotropic cooperativity. Enzyme inactivation led to an increase in mass of the apo-CYP2B4 by 218 Da as determined by ESI-LC/MS, consistent with covalent protein modification. The modified CYP2B4 was purified to homogeneity and its structure determined by X-ray crystallography. The structure showed that 9EP is covalently attached to the Oγ of Thr 302 via an ester bond, which is consistent with the increased mass of the protein. The presence of the bulky phenanthrenyl ring resulted in inward rotations of Phe 297 and Phe 206 leading to a compact active site. Thus, binding of another molecule of 9EP in the active site is prohibited. However, results from the quenching of 9EP fluorescence by unmodified or 9EP-modified CYP2B4 revealed at least two binding sites with distinct affinities, with the low affinity site being the catalytic site and the high affinity site on the protein periphery. Computer-aided docking and MD simulations with one or two ligands bound revealed that the high affinity site is situated at the entrance of a substrate access channel surrounded by the F' helix, β1/β2 loop and β4 loop and functions as an allosteric site to enhance the efficiency of activation of the acetylenic group of 9EP and subsequent covalent modification of Thr 302.

Human microsomal cytochromes P450 (CYPs or P450s) metabolize nearly ~70% of clinically used drugs (1). Evolved to clear a variety of xenobiotic chemicals from the human body, drug-metabolizing P450s are promiscuous in nature and exhibit a wide range of

[1]Coordinates and structure factors of 9EP-modified CYP2B4 were deposited in the Protein Data Bank with the accession code of 3UAS.

[*]**Corresponding Author**phollen@umich.edu; Tel: 734-764-8166; Fax: 734-763-5378 .
[†]Department of Molecular Biology, The Scripps Research Institute, La Jolla, CA 92037, USA

Author Contributions The manuscript was written through contributions of all authors. All authors have given approval to the final version of the manuscript.

Notes The authors declare no competing financial interest.

ASSOCIATED CONTENT Supporting information Two figures are included in the Supplemental Material. This material is available free of charge via the Internet at http://pubs.acs.org.

catalytic efficiencies. Since the early 1970s, kinetic studies of drug metabolism have revealed that a growing number of P450-catalyzed reactions do not follow the classic Michaelis-Menten model. Instead, both homotropic and heterotropic cooperativity have been documented for a number of mammalian P450s, including CYP3A4, 2C9, 2B4, 2D6, 1A2, and 2E1, among which the cooperativity of CYP3A4 is best studied (for reviews, see (2-4)). These “non Michaelis-Menten” kinetics or atypical kinetics pose great challenges in predicting the pharmacokinetics of drugs.

Because of its pharmacological importance, the atypical kinetics of P450s has been extensively studied over the past three decades. Contrasting models have been put forward to interpret the mechanisms by which cooperativity occurs. A static “space-filling” model proposes that simultaneous binding of two substrate molecules may result in one substrate being more favorably oriented for productive catalysis (5, 6). Alternatively, the allosteric model proposes modulations of P450 activities by effectors that bind at remote allosteric site(s) and induce conformational changes (7-9). X-ray crystallographic studies of P450s have previously shown that multiple substrates or inhibitors are bound at distinct binding sites (10-13). A recent study using fluorescence resonance energy transfer (FRET) has identified a high affinity peripheral binding site in CYP3A4 that modulates substrate binding through an allosteric conformational transition (8).

Despite numerous reports of the cooperativity of P450-catalyzed reactions, there are no reports on cooperativity during mechanism-based inactivation of P450s. It is not uncommon that metabolism of xenobiotic compounds by P450s generates reactive metabolites capable of covalent modification of critical cellular components. The reactive metabolites produced by P450s may in fact result in inactivation of P450s via a process referred to as mechanism-based inactivation (14). Inactivation of P450s can have significant ramifications for drug toxicity, chemical carcinogenesis and adverse drug interactions. The withdrawal of several pharmaceutical drugs from market such as mibefradil and troglitazone has been linked to the formation of reactive metabolites by P450s.

Aromatic acetylenes represent a class of mechanism-based inactivators (MBIs) with defined chemistries and favorable binding energies to the hydrophobic active sites of P450s. They are useful probes for interrogating the structure, function, and mechanism of action of P450s. Potent acetylenic MBIs with low partition ratios are particularly desirable, as homogenously modified P450 enzymes can be obtained for various functional and structural analyses. For instance, we previously determined the first crystal structure of a covalently modified CYP2B4, which provides unequivocal evidence for the covalent modification of the highly conserved Thr 302 residue and elucidates the mechanism by which this acetylene inactivates CYP2B4 (15).

Here we report the mechanism-based inactivation of CYP2B4 by 9-ethynylphenanthrene (9EP). Our results demonstrate that 9EP is a potent MBI of CYP2B4 with a partition ratio and k_{inact} of 0.2 and 0.25 min^{-1}, respectively. Interestingly, inactivation of CYP2B4 by 9EP exhibits sigmoidal kinetics with a Hill coefficient of 2.5 and S_{50} of 4.5 μM, which indicate positive homotropic cooperativity. Through the combined use of fluorescence quenching, X-ray crystallography and computer-aided modeling, we have demonstrated that the homotropic cooperativity is due to allosteric modulations of the conformation of the 9EP bound in the active site leading to more efficient catalysis and inactivation.

EXPERIMENTAL PROCEDURES

Materials

All chemicals used are of highest purity available unless otherwise specified. NADPH and catalase were purchased from Sigma-Aldrich Inc. (St. Louis, MO), trifluoroacetic acid (TFA) was purchased from Pierce Chemicals (Rockford, IL), and 7-ethoxy-4-trifluoromethylcoumarin (7-EFC) was purchased from Invitrogen Molecular Probes (Eugene, OR). The nonionic detergent Cymal-5 was purchased from Anatrace (Maumee, OH). Carbon monoxide with purity > 99.5% was purchased from Cryogenic Gas (Detroit, MI). An N-terminal truncated wild type form of CYP2B4 (CYP2B4dH), full-length P450 reductase (CPR) and cytochrome b_5 (cyt b_5) were over-expressed and purified from bacterial C41(DE3) cells as previously described (16).

Characterization of the mechanism-based inactivation of CYP2B4 by 9EP

The kinetics for the inactivation of CYP2B4 by 9EP were determined in 50 mM potassium phosphate (KPi) buffer (pH 7.4) using a 96-well microtiter plate as previously described (17). The reaction was maintained at 30 °C with orbital shaking at 500 rpm using a thermal incubator (THERMOstar 45, BMG LabTech, Cary, NC). CYP2B4, CPR and cyt *b5* were reconstituted for 30 min at room temperature and then diluted with 50 mM KPi buffer (pH 7.4) to give a final concentration of 0.5 (CYP2B4), 1.0 (CPR), and 1.0 (cyt *b5*) μM. The concentrations of 9EP were varied between 0-5 μM. Inactivation of CYP2B4 was initiated by the addition of NADPH to a final concentration of 1 mM. At designated times, aliquots (6 μL) of the primary reaction mixture were transferred to a secondary reaction mixture (0.15 ml) that contained 0.1 mM 7-EFC and 0.3 mM NADPH in 50 mM KPi buffer (pH 7.4). The secondary reactions were terminated after incubation for 10 min by the addition of 50 μL of ice-cold acetonitrile. Fluorescent emission from the 7-hydroxy-4-trifluoromethylcoumarin (7-HFC) product was measured at 520 nm with excitation at 410 nm and its intensity was used to calculate the activity remaining. The results were expressed as percentage of the control sample that did not contain 9EP. To obtain kinetic parameters, the dependence of the v_{obs} vs [9EP] was fit to a Michaelis-Menten or an allosteric sigmoidal model as shown in Eq. 1 using GraphPad Prism 6 (GraphPad Software Inc, La Jolla, CA):

$$V=\frac{k_{inact} \times S^n}{S_{50}^n+S^n} \quad \text{(Eq.1)}$$

, where v is the velocity, k_{inact} is the rate constant for inactivation, S is the concentration of MBI, S_{50} is the inhibitor concentration showing a half-maximal velocity, and n is a measure of cooperativity (18).

To determine the partition ratio, the primary reaction mixture containing CYP2B4, CPR, cyt *b5*, catalase, and various concentrations of 9EP was incubated as indicated previously except that incubation of the primary reaction mixture was allowed to proceed for 30 min until the mechanism-based inactivation was complete. The partition ratio was then determined based on the activities remaining as previously described (19).

Analysis of the molecular mass of the 9EP-modified CYP2B4 using ESI-LC/MS

The molecular mass of the 9EP-modified CYP2B4 was analyzed by ESI-LC/MS using an ion-trap mass spectrometer (LCQ DecaXP, ThermoScientific, Waltham, MA) as previously described (20). Following incubation with 9EP in the presence of 1 mM NADPH for 5 min at 30 °C, an aliquot (50 μL) of the primary reaction mixture was applied to a reverse-phase C3 column (2 × 150 mm, 5 μm, Agilent Technologies, CA). CYP2B4 was separated from the other reaction components with a binary solvent system consisting of 0.1% TFA in water

(Solvent A) and 0.1% TFA in acetonitrile (Solvent B) using the following gradient: 30% B for 5 min, linearly increased to 90% B in 20 min, and held at 90% B for 30 min. The flow rate was 0.25 mL/min. The molecular masses of the unmodified and 9EP-modified CYP2B4 were determined by deconvolution of the apoprotein charge envelopes using the Bio-works software (Thermo Scientific, Waltham, MA).

X-ray crystallographic studies of 9EP-modified CYP2B4

To gain further atomic level insights into the potent inactivation of CYP2B4 by 9EP, we determined the crystal structure of the modified CYP2B4 using X-ray crystallography. In order to obtain sufficient quantities of 9EP-modified CYP2B4 for X-ray crystallographic studies, the inactivation reaction of CYP2B4 by 9EP was scaled up to use 500-1000 nmoles of CYP2B4. Labeling of CYP2B4 with 9EP and purification of the labeled CYP2B4 were performed as previously described (15). The purified labeled protein was then concentrated with a VIVASPIN 2 protein concentrator (cutoff 30K, Sartorius Stedim Biotech, Germany) to 270 μM in 50 mM KPi buffer (pH 7.4 at 4 °C) containing 500 mM NaCl, 500 mM sucrose, 1 mM EDTA, and 0.2 mM dithiothreitol. The concentrated protein solution was supplemented with 4.8 mM Cymal-5 and 0.028% (w/v) 232-chol and allowed to equilibrate for approximately 15 min before mixing with the crystallization reagents. Screening for protein crystallization conditions was performed by sitting drop vapor diffusion using the Wizard II high throughput kit from Emerald Biosystems (Bainbridge Island, WA) by mixing equal volumes of protein solution and well solution. Drops were equilibrated against the well solution at 18 °C and crystals grew over the course of a week in drops containing 0.1 M Tris (pH 7.0), 20% (w/v) PEG 3000, and 0.2 M calcium acetate. Crystals were briefly transferred to a mother liquor solution supplemented with 335 mM sucrose before flash freezing in liquid nitrogen. Data were collected on a Bruker X8 Prospector diffractometer. The data were indexed, integrated, scaled and merged using the Bruker Proteum software suite. Phases were obtained by molecular replacement using the previously determined 2B4–4CPI complex (PDB ID 1SUO) (with the inhibitor molecule removed from the coordinates) in Phaser (21). The structure solution was found in space group $P3_121$ containing 61.9% solvent, assuming one molecule per asymmetric unit. The initial model was subjected to simulated annealing followed by restrained refinement in PHENIX (22) to remove model bias. Model building was performed in Coot (23) using both 2*Fo-Fc* and *Fo-Fc* electron density maps contoured to 1-σ and 3-σ, respectively. The covalent ligand definition file was generated using JLigand (24). The model was modified to fit the electron density and refined in an iterative manner until a final R-factor of 24.5 % and an R_{free} of 29.6 % were reached. Coordinates and structure factors were deposited in the Protein Data Bank (accession code 3UAS). Data collection and refinement statistics are shown in Table 1.

Fluorescence quenching upon binding of 9EP to unmodified and 9EP-modified CYP2B4

Quenching of the 9EP fluorescence by CYP2B4 was utilized to investigate the binding of 9EP to CYP2B4. Fluorescence emission from 9EP was measured using a Synergy2 multi-mode microplate reader with an excitation filter 310/20 nm, an emission filter 380/20 nm, and a 365 nm cutoff dichroic mirror (BioTek, Winooski, VT). Aliquots (0.2 ml) of the 9EP solution (0.5 μM in 0.1 M KPi, pH 7.4) were dispensed into 96-well plates. Equal volumes (10 μL) of protein stock solutions were then added to each well to give final protein concentrations in the range of 0-2 μM. The samples were incubated at ambient temperature in the dark for 10 min, and then fluorescence emission from 9EP was measured and the final results were averaged from four separate measurements. To ensure that unmodified and 9EP-modified CYP2B4 contained the same amount of the heme, their concentrations were determined using the pyridine hemochromogen assay as reported previously (25).

Computer-aided docking and MD simulations of 9EP binding to CYP2B4

To identify the binding sites for 9EP in CYP2B4, 9EP was docked as a flexible ligand to the rigid CYP2B4 receptor using Autodock 4.0 (26). The coordinates of CYP2B4 were obtained from the Protein Data Bank (PDB ID: 1SUO) whereas the coordinates of 9EP ligand were constructed using the ChemBioOffice software suite (CambridgeSoft, MA). To search for all possible binding cavities both in the interior and exterior of CYP2B4, a relatively large potential energy grid with a size of 47 × 47 × 47 Å was used for initial dockings to generate the coordinates for the CYP2B4-9EP complex for subsequent MD simulations. Gasteiger partial charges were assigned to proteins using AutoDockTools while the partial charges obtained from DFT calculations were assigned to the ferric heme (see below). The docking parameters were as follows: population size, 150; number of evaluations, 2.5×10^6; mutation rate, 0.2. A total of 100 poses were generated and they were clustered using a root-mean-square-deviation (r.m.s.d) of 2.0 Å.

MD simulations were performed in explicit solvent under periodic boundary conditions using the Amber 11 software package (27). The Amber force field was used to generate the parameter and topology files for the complex. The heme moiety was also included in the MD simulations as a penta-coordinated ferric heme ligated to Cys 436. The thiolate-ligated ferric heme was parameterized by Dr. Dan Harris as previously reported (28). The 9EP ligand was parameterized with a general Amber force field (GAFF) using Antechamber tools.

The complex was solvated with TIP3 water with the protein being 12.0 Å away from the periodic boundary. The solvated system was neutralized by the addition of chloride ions. Additional sodium and chloride ions were randomly distributed into the solvated system to give a concentration of 0.1 M NaCl. The entire system consisted of ~ 54000 atoms. Prior to MD simulations the energy of the system was minimized using a combination of energy minimization algorithms including 5000 steps of steepest descent followed by 5000 steps of conjugate gradient. The energy-minimized system was then heated to 310 K under constant volume. After a brief equilibrium for 300 ps, unrestricted MD production was performed under NPT conditions (T = 310 K, P = 0.1 MPa) for 10 ns with weak coupling thermostat and barostat. The cut-off distance for non-bonded interactions was 10 Å and the motions of all hydrogen atoms were restricted with the SHAKE algorithm. Trajectories from the MD simulations were analyzed using the ptraj program.

RESULTS

Kinetics of the mechanism-based inactivation of CYP2B4 by 9EP

Metabolism of 9EP by CYP2B4 led to a rapid loss of 7-EFC *O*-deethylase activity. As shown in Figure 1A, this loss in activity was time-, concentration- and NADPH-dependent. Although the rate of inactivation was linear over time, it exhibited a sigmoidal dependence on the concentrations of 9EP (Figure 1B). As such, the data fit poorly to a Michaelis-Menten model (dashed line, Figure 1B) but well to a sigmoidal model as defined in Eq. 1 (solid line, Figure 1B), which gave a k_{inact} of 0.25 min^{-1} inact , S_{50} of 4.5 μM, and n (Hill coefficient) of 2.5. Although n has no physical meaning, it is a measure of enzyme cooperativity. A range of n values from 1.3 to 3.6 have been reported for various P450-catalyzed reactions showing positive cooperativity (29-31). The observed n value of 2.5 for the mechanism-based inactivation of CYP2B4 by 9EP is within this range. The sigmoidal kinetics observed here is in striking contrast to the typical hyperbolic kinetics that have been previously observed for the MBIs of P450s including many acetylenic inactivators (16, 32, 33). To assess the potency, the partition ratio for the mechanism-based inactivation of CYP2B4 by 9EP was also determined as shown in Figure 1C. The two solid lines intercepted with the x-

axis at 1.2 as indicated by an arrow. Subtraction of one molecule of 9EP that is required to inactivate CYP2B4 from the intercept gave the partition ratio of 0.2±0.03 (34). This very low partition ratio indicated that the reactive intermediate of 9EP inactivates CYP2B4 very effectively without leaving the active site.

Effects of mechanism-based inactivation by 9EP on CYP2B4

The effects of the mechanism-based inactivation were evaluated by examining possible alterations in both the apo-protein and the heme of CYP2B4. The molecular mass of the inactivated CYP2B4 was analyzed using ESI-LC/MS, and the results are shown in Figure 2. The control sample of CYP2B4 showed a molecular mass of 53958 Da, which is within 0.013% of 53948 Da as we reported previously for CYP2B4 (16). In contrast, the inactivated CYP2B4 showed an increase in mass of 218 Da. This increase is equivalent to the mass of one 9EP (202 Da) plus one oxygen atom. The mass of the unmodified CYP2B4 was not observed in the inactivated sample, indicating that the CYP2B4 was completely labeled by 9EP.

We also examined the effect of mechanism-based inactivation by 9EP on the heme moiety by measuring the CO-detectable heme. As shown in Figure 3, the 9EP-modified CYP2B4 showed a loss of the CO-detectable heme of approximately 50% compared with the control sample. Interestingly no loss of the native heme was observed when the inactivated protein was analyzed by HPLC (data not shown).

Crystallographic studies of 9EP-modified CYP2B4

The MOLPROBITY analysis (35) of the deposited structure revealed the score of 100th percentile among structures of comparable resolutions. The Ramachandran analysis is presented in Table 1. Both analyses indicated that the determined crystal structure has good quality. The final model of the structure contains protein residues from 28 to 492. As shown in Figure 4A, the overall fold of the 9EP-modified CYP2B4 is very similar to that of the CYP2B4 complexed with 4-(4-chlorophenyl)imidazole (CPI) (36). Both structures exhibit closed conformations and the backbone root-mean-square (r.m.s) is only 0.33 Å. An unbiased electron density attributed to the 9EP moiety was observed above the heme plane. As observed in the crystal structure of CYP2B4 inactivated by *tert*-butylphenylacetylene (tBPA) (15), the terminal C16 carbon of the acetylenic group of the 9EP moiety is covalently attached to the Oγ atom of the highly conserved Thr302 residue via an ester bond. Those residues within 5 Å of the 9EP moiety are mostly hydrophobic residues such as Ile 114, Phe 115, Phe 206, Ile 209, Phe 297, Ala 298, Ile 363, Val 367 and Val 477, as well as residues Ser 210, Glu 301, Thr 302 and Gly 478 as shown in Figure 4B. In particular, Phe 206, Phe 297 and Val 477 are nearly in van der Waals contact with the phenanthrenyl ring, presumably due to strong hydrophobic interactions. Compared with the active site residues observed in the closed conformation of tBPA-modified CYP2B4, Phe 297 and Val 477 are rotated further toward the phenanthrenyl ring resulting in a more compact active site. An overlay of the active site structures of CYP2B4 modified by tBPA or 9EP showing all of the amino acid residues within 5 Å of both ligands is provided in the Supplemental Materials (Figure S1). It is noteworthy that tBPA-modified CYP2B4 exhibited both open and closed conformations, whereas the 9EP-modified CYP2B4 was observed only in the closed conformation. Therefore, it is highly unlikely that the active site of CYP2B4 could accommodate two 9EP ligands simultaneously.

Fluorescence quenching upon binding of 9EP to CYP2B4

To better understand the origin of the sigmoidal kinetics for the mechanism-based inactivation of CYP2B4, the binding of 9EP to CYP2B4 was investigated using fluorescence quenching. As shown in Figure 5, addition of the 9EP-modified CYP2B4 to 0.5 μM 9EP led

to a sharp decrease in the fluorescence emission (open circle). This concentration-dependent decrease in fluorescence emission leveled off at 47% when approximately 0.5 μM 9EP-modified CYP2B4 was added. Thus it appears that 9EP forms a tight 1:1 complex with the 9EP-modified CYP2B4. It is noteworthy that the phenanthrenyl moiety covalently attached to Thr302 emits no fluorescence upon being excited at 310 nm (see Figure S2 in the Supplemental Materials). Since the active site of the 9EP-modified CYP2B4 does not have sufficient space to accommodate two 9EP molecules, it can be concluded that the quenching of the 9EP fluorescence by 9EP-modified CYP2B4 results from the binding of one 9EP ligand to a peripheral site. To further confirm the existence of a peripheral binding site, fluorescence quenching by unmodified CYP2B4 was determined. As observed with 9EP-modified CYP2B4, titration of 9EP with unmodified CYP2B4 also led to initial sharp decrease in fluorescence emission (solid square, Figure 5). However, unlike the 9EP-modified CYP2B4, this decrease did not level off at 0.5 μM concentration, but rather continued slowly at increasing concentrations of unmodified CYP2B4. This biphasic quenching suggests that at least two binding sites for 9EP exist with distinct affinities.

To ensure that the quenching of fluorescence was due to specific interactions of the 9EP with CYP2B4, we also examined the fluorescence emission of 9EP in the presence of cyt *c*. Cyt *c* is analogous to P450s with respect to pI values and the presence of the ferric heme moiety and therefore it serves as a proper control. The results showed that less than 10% of the fluorescence emission was quenched by 2 μM cyt *c* (solid triangle, Figure 5)

Computer-aided docking and MD simulations

Computer-aided docking was used to explore the potential binding sites for 9EP. Results from the energy-based docking of 9EP to CYP2B4 revealed several potential binding sites for 9EP. As summarized in Table 2, the binding energy for these sites is in the range of −8.80 to −7.09 kcal/mol. The cluster with the lowest binding energy is located in the active site and is composed of 21 poses (21%). However, the majority of the poses (45%) are clustered in a binding pocket located on the periphery of CYP2B4, approximately 17 Å from the heme iron. This site is referred to as the distal site from this point forward. The third largest cluster consists of 14 poses, but these are bound to a site on the proximal side of the heme. These poses are not expected to play any role in catalysis in the presence of CPR because it is well documented that CPR is bound to the proximal side of P450s (37). Therefore this cluster of ligands was excluded from subsequent MD simulations.

To examine the stability of the bound 9EP ligand, the CYP2B4-9EP complex was subjected to a 500 ps MD simulation. The results showed that only the 9EP bound in the active site and the distal site were stable during the MD simulations, while the 9EP molecules bound elsewhere escaped from the binding sites (data not shown).

To further explore how the two binding sites may interact to affect the catalysis, we carried out two independent MD simulations under identical conditions. In the first simulation the 9EP ligand was bound in the active site to form a binary complex of CPY2B4-9EP, while in the second simulation 9EP ligands were bound to both the active site and the distal site to form a tertiary complex of CYP2B4-9EP^2. Extended MD simulations showed that the conformation of the 9EP ligand in the binary complex was unstable. As shown in Figure 6A, the distances from the heme iron (Fe) to the terminal C16 carbon of the acetylenic group of 9EP and from the C16 to the Oγ of the Thr302 side chain (OG1) are sharply increased at ~8 ns, indicative of a conformational transition of the 9EP ligand in the active site. In marked contrast, both distances remained steady in the tertiary complex as shown in Figure 6B.

The structural changes accompanying this conformational transition observed in the binary complex are depicted in Figure 7. The initial conformation of 9EP in the binary complex

shares great similarity to that observed in the crystal structure of the 9EP-modified CYP2B4. Namely the C16 carbon is in close proximity to both the heme iron and Thr302. Residues within 5 Å of the 9EP include a number of hydrophobic atoms from Phe 206, Phe 297, Phe 115, Val 480, Val 367, Val 363, Val 477, Val 104, Leu 363, and Ile 209. Not only does the 9EP ligand interact with residues in the I-helix, B/C loop, and K-L loop, it also interacts with several residues from the F-helix and the β4 loop near the C-terminus. The trajectory of the binary complex obtained at 8.2 ns shows that the 9EP ligand rotates ~120° away from the heme iron, resulting in nearly 3-fold increases in the Fe-C16 and C16-OG1 distances. Furthermore, strong hydrophobic interactions between 9EP and surrounding residues are partially lost. In particular the interactions between 9EP and the residues located in the F-helix and β4 loop no longer exist. This is more clearly shown in Figure 7C where the two trajectories were superimposed. The backbone r.m.s between these two trajectories is 1.36 Å, indicating significant structural differences. Most notably the major structural changes were observed in the F-, F'-, and C-helices and β4 loop where the axis of the F-helix rotated ~ 5° away from the heme plane, and the β4 loop retracted from the active site, leading to a more open active site. In contrast, the 9EP ligand bound in the active site of the tertiary complex remained remarkably stable during the course of MD simulations. The active site 9EP did not undergo any large conformational transitions as evidenced by relatively constant distances between the Fe-C16 and C16-OG1. The averaged distances between Fe-C16 and C16-OG1 are approximately ~ 5 Å. In particular, the interactions between 9EP and the residues Phe 206, Ile 209, and Val 477 are maintained. These striking differences in the orientations of the active site 9EP ligand underscore the important role of the peripheral 9EP ligand in modulating P450 conformations and ligand binding in the active site.

DISCUSSION

In this work we have demonstrated that 9EP is a potent MBI of CYP2B4. The halftime for the mechanism-based inactivation of CYP2B4 is ~ 2.7 min. In addition, the low partition ratio of 0.2 for the inactivation indicates that the reactive metabolite of 9EP inactivates CYP2B4 without leaving the active site. This is consistent with our observation that no glutathionyl adducts of 9EP were detected from the reaction mixture (data not shown). Furthermore we have elucidated the mechanism by which 9EP inactivates CYP2B4 through allosteric modulation.

Analysis of the 9EP-modified CYP2B4 by MS suggest that 9EP inactivates CYP2B4 via covalent modification of the highly conserved Thr 302 residue, similar to the mechanism-based inactivation of CYP2B4 by tBPA, another potent aromatic MBI. It is expected that metabolism of 9EP by CYP2B4 generates a reactive ketene intermediate that in turn forms a covalent ester bond with the Oγ atom of Thr 302. Covalent bonding between the ketene intermediate and the Oγ atom of Thr 302 would be expected to increase the molecular mass of CYP2B4 by 218 Da, equivalent to the molecular mass of 9EP (202 Da) plus one oxygen atom. This is in complete agreement with our analyses of the molecular masses of the control and 9EP-modified CYP2B4 (see Figure 2). The potent inactivation of CYP2B4 by 9EP resulting from covalent modification of a single amino acid residue provides a unique opportunity to purify the modified CYP2B4 to homogeneity for subsequent studies of the crystal structure of the 9EP-modified CYP2B4.

The crystal structure of 9EP-modified CYP2B4 unequivocally confirmed that the 9EP moiety forms a covalent bond with the highly conserved Thr 302. The terminal carbon C16 of 9EP is covalently attached to the Oγ atom of the side chain Thr 302 with a C-O bond length of 1.5 Å. Furthermore, the crystal structure also revealed that the 9EP-modified CYP2B4 adopts a closed conformation with the overall fold similar to that of CYP2B4 complexed with the inhibitor CPI (see Figure 4). Although covalent modification of Thr 302

by 9EP does not seem to have altered the overall structure of CYP2B4, subtle changes in the active site architecture are noted. The major changes are the inward rotation of Phe 297, Phe 206, and Val 477, which bring these residues nearly in van der Wales contact with the phenanthrenyl rings. This results in a more compact active site packed with a number of hydrophobic residues including Phe 115, Phe 297, Phe 206, Val 477, Val 367, Ile 363, Ile 209, Ala 298 in addition to Glu 301 and Ser 210. The tightly packed active site precludes the possibility of the binding of a second bulky 9EP molecule. This is further supported by the alteration in the CO difference spectra (see Figure 3). The 9EP-modified CYP2B4 lost ~50% of the CO-detectable heme even though no modification of the native heme was observed by HPLC analysis. This decrease in the intensity of the CO difference spectra is likely due to steric hindrance of CO binding from the bulky phenanthrenyl ring and the associated changes in polarity in the active site. We reported previously that covalent modification of Thr 302 of CYP2B4 by tBPA significantly affects the stretching frequencies of the Fe-CO mode and the C-O mode (38). Presumably, the presence of the bulkier phenanthrenyl ring would have a more significant impact on the binding of CO and other ligands.

The most striking feature of the mechanism-based inactivation of CYP2B4 by 9EP is the sigmoidal kinetics. Unlike tBPA, 9EP exhibits homotropic cooperativty for the inactivation. Our results provide convincing evidence for allosteric modulation of the catalytic oxidation of 9EP. First, measurements of fluorescence quenching clearly indicate the existence of low and high affinity binding sites for 9EP (see Figure 5). The fact that only the high affinity site was observed in 9EP-modified CYP2B4 strongly suggests that this site is located on the periphery of CYP2B4 rather than in the active site. As such, the low affinity site must be then in the active site. Both the fluorescence quenching and the analyses of the crystal structure of the 9EP-modified CYP2B4 do not support simultaneous binding of multiple 9EP substrates in the active site. Second, MD simulation of both the binary and tertiary complexes of CYP2B4 underscores the importance of conformational plasticity in modulating the conformations of the active site 9EP. We reported previously that the efficiency and potency for the covalent modification of the Thr 302 of CYP2B4 by acetylenes is due to the proximity of the terminal carbon of the acetylenic group to both the heme iron and the Oγ atom of Thr 302 (15, 16, 39). This proximity allows efficient activation of the acetylenic group by P450 to form the ketene intermediate followed by facile electrophilic attack from the Oγ atom of Thr 302. Stabilization of this geometry or active conformation would undoubtedly facilitate the mechanism-based inactivation. Results from the MD simulations demonstrate that the active conformation of 9EP is stable during the course of the simulations only if the allosteric site is occupied by another 9EP (see Figure 6B). Otherwise the active site 9EP undergoes a conformational transition leading to the acetylenic group drifting away from the heme iron.

Our results from the MD simulations further illustrated that this conformational transition of the active site 9EP is due to the increased conformational plasticity of CYP2B4 in the absence of the allosteric 9EP ligand. Specifically the motions of the F-helix and β4 loop are largely responsible. Comparison of the residues within 5 Å of the active site 9EP between the initial structure and the one obtained at 8.2 ns (see Figure 7A and 7B) shows that the 9EP in the active site no longer interacts with Phe 206, Ile 209, Ser 210 of the F-helix and Val 480 and Val 477 of the β4 loop. In marked contrast, when the allosteric site is occupied, the structure of CYP2B4 is more stable, particularly in the regions of F-helix and β4 loop. As such, the interactions of the active site 9EP with Phe 206, Ile 209, Ser 210, and Val 477 are maintained to stabilize the active conformation of the 9EP bound in the catalytic site. The important roles of the F-helix and β4 loop in P450 catalysis have been documented in a large body of literature (40-46). It is noteworthy that double mutation of L211F/D214E in this region abolishes homotropic cooperativity of CYP3A4 (29). Furthermore, we have

reported that the Cys 475 located in the β4 loop is an integral part of the substrate access channels (46).

The allosteric site for 9EP is located on the distal side of the heme and surrounded by the β1/β2 loop, B/C loop, F'-helix and β4 loop near the C-terminus. This binding pocket has been observed in a number of X-ray crystal structures of P450s including CYP2B4 (11, 12), 2B6 (12), 245A1 (P450 StaP) (13), and 21A2 (10). It was found that one of three molecules of the antifugal drug bifonazole is bound to CYP2B4 at this site and one of the three chromopyrrolic acid molecules is bound to CYP245A1 in a similar pocket. Recently, two independent studies have reported simultaneous binding of two substrates in the crystal structures of CYP2B4 and CYP2B6 (12) and CYP21A2 (10) with one of the substrates being trapped in a substrate access channel and the other bound in the active site. The identified channel extends from the active site to a cleft on the surface surrounded by the β1/β2-loop, B/C-loop, F'-helix and β4 loop. The allosteric site for 9EP shares great similarity to the cleft identified by these studies, although the exact pockets differ slightly due to the highly plastic nature of the surrounding structural elements. Our MD simulations showed that the 9EP bound at the allosteric site samples a number of conformations due to its partial exposure to the surface, which would facilitate ligand entrance into the access channel. Several residues within 5 Å of the allosteric 9EP such as Leu 43, Leu 51, Leu 70, Gln 215, Leu 219, and Val 477 were also identified in the distal binding pocket for the amlodipine in CYP2B4, although amlopidine is less surface-exposed (12).

The averaged distance between the two 9EP ligands in the tertiary complex of CYP2B4 and 9EP is approximately 12 Å. This raises an intriguing question: how does the allosteric regulation of P450 catalysis occur over this relatively long distance? Our results from the MD simulations seem to suggest that this is due to a more rigid structure of CYP2B4 induced by the binding of a second 9EP at the allosteric site. It is well established that the structures of mammalian P450s are highly flexible, particularly in the F- and G-helices, F/G-loop, and B/C loop regions. Large conformational changes in these regions have been observed in the crystal structures of CYP2B4 and tBPA-modified CYP2B4, leading to open conformations of the active sites (11, 15, 47). Unconstrained access to the active site would increase uncoupling reactions and attenuate catalytic specificity. Binding of the 9EP to the allosteric site significantly limits the motions of the F-helix and β4 loop resulting in favorable orientation of the 9EP in the active site for efficient catalysis and inactivation. This is consistent with a recent report that binding of fluorol-7GA, a model substrate for CYP3A4, at a peripheral site between the F and G helices affects the binding of substrate in the active site through a conformational transition (8). Further studies are under way to investigate the roles of specific amino acid residues in these allosteric modulations using site-specific mutagenesis.

CONCLUSIONS

In conclusion, we have demonstrated that 9EP is a potent MBI of CYP2B4 and it inactivates CYP2B4 through covalent modification of the highly conserved Thr 302 residue. Furthermore, we have shown that the homotropic cooperativity observed during the mechanism-based inactivation of CYP2B4 by 9EP is due to allosteric modulation of the P450 catalysis through the binding of a second 9EP ligand on the protein periphery. Specifically, MD simulations of the tertiary complex of CYP2B4 and 9EP reveal that the binding of the 9EP to the allosteric site significantly limits the motions of the F-helix and β4 loop resulting in favorable orientation of the 9EP in the active site for efficient catalysis and inactivation.

Supplementary Material

Refer to Web version on PubMed Central for supplementary material.

Acknowledgments

The authors are grateful to Dr. Dan Harris for providing us with the parameters for the ferric thiolate-ligated heme and Dr. Mathew Young for use of his computer clusters for MD simulations. We thank Mrs. Hsia-lien Lin for providing purified P450 reductase and cyt b_5.

Funding Sources This work is, in whole or in part, is supported by NIH grants CA016954 to Paul F. Hollenberg, ES003619 to James R. Halpert, Louisiana Cancer Research Consortium support and NIH-RCMI grant 8G12MD007595-04 to Maryam Foroozesh, GM077430 to Yoichi Osawa, AA020090 to Haoming Zhang, and GM098538 to Qinghai Zhang

ABBREVIATIONS

7-EFC	7-ethoxy-4-trifluoromethylcoumarin
7-HFC	7-hydroxy-4-trifluoromethylcoumarin
9EP	9-ethynylphenanthrene
CPR	NADPH-cytochrome P450 reductase
cyt b5	cytochrome *b5*
ESI-LC/MS	electrospray ionization liquid chromatography mass spectrometry
MBI	mechanism-based inactivator
MD	molecular dynamics
P450	cytochrome P450
TFA	trifluoroacetic acid
CPI	4-(4-chlorophenyl)imidazole
232-chol	3α,7α,12α-tris[(β-D-maltopyranosyl)ethyloxy]cholane

REFERENCES

1. Guengerich FP. Cytochrome P450 and chemical toxicology. Chem. Res. Toxicol. 2008; 21:70–83. [PubMed: 18052394]
2. Sligar SG, Denisov IG. Understanding cooperativity in human P450 mediated drug-drug interactions. Drug Metab Rev. 2007; 39:567–579. [PubMed: 17786639]
3. Davydov DR, Halpert JR. Allosteric P450 mechanisms: Multiple binding sites, multiple conformers or both? Expert Opin Drug Metab Toxicol. 2008; 4:1523–1535. [PubMed: 19040328]
4. Tracy TS. Atypical cytochrome P450 kinetics: Implications for drug discovery. Drugs R D. 2006; 7:349–363. [PubMed: 17073518]
5. Dabrowski MJ, Schrag ML, Wienkers LC, Atkins WM. Pyrene-Pyrene complexes at the active site of cytochrome P450 3A4: Evidence for a multiple substrate binding site. J. Am. Chem. Soc. 2002; 124:11866–11867. [PubMed: 12358527]
6. Ekroos M, Sjogren T. Structural basis for ligand promiscuity in cytochrome P450 3A4. Proc. Natl. Acad. Sci. USA. 2006; 103:13682–13687. [PubMed: 16954191]
7. Tsalkova TN, Davydova NY, Halpert JR, Davydov DR. Mechanism of interactions of α-naphthoflavone with cytochrome P450 3A4 explored with an engineered enzyme bearing a fluorescent probe. Biochemistry. 2007; 46:106–119. [PubMed: 17198380]

8. Davydov DR, Rumfeldt JA, Sineva EV, Fernando H, Davydova NY, Halpert JR. Peripheral ligand-binding site in cytochrome P450 3A4 located with fluorescence resonance energy transfer (FRET). J. Biol. Chem. 2012; 287:6797–6809. [PubMed: 22194603]
9. Isin EM, Guengerich FP. Kinetics and thermodynamics of ligand binding by cytochrome P450 3A4. J. Biol. Chem. 2006; 281:9127–9136. [PubMed: 16467307]
10. Zhao B, Lei L, Kagawa N, Sundaramoorthy M, Banerjee S, Nagy LD, Guengerich FP, Waterman MR. Three-dimensional structure of steroid 21-hydroxylase (cytochrome P450 21A2) with two substrates reveals locations of disease-associated variants. J. Biol. Chem. 2012; 287:10613–10622. [PubMed: 22262854]
11. Zhao Y, White MA, Muralidhara BK, Sun L, Halpert JR, Stout CD. Structure of microsomal cytochrome P450 2B4 complexed with the antifungal drug bifonazole: Insight into P450 conformational plasticity and membrane interaction. J. Biol. Chem. 2006; 281:5973–5981. [PubMed: 16373351]
12. Shah MB, Wilderman PR, Pascual J, Zhang Q, Stout CD, Halpert JR. Conformational adaptation of human cytochrome P450 2B6 and rabbit cytochrome P450 2B4 revealed upon binding multiple amlodipine molecules. Biochemistry. 2012; 51:7225–7238. [PubMed: 22909231]
13. Makino M, Sugimoto H, Shiro Y, Asamizu S, Onaka H, Nagano S. Crystal structures and catalytic mechanism of cytochrome P450 stap that produces the indolocarbazole skeleton. Proc. Natl. Acad. Sci. USA. 2007; 104:11591–11596. [PubMed: 17606921]
14. Hollenberg PF, Kent UM, Bumpus NN. Mechanism-based inactivation of human cytochromes P450s: Experimental characterization, reactive intermediates, and clinical implications. Chem. Res. Toxicol. 2008; 21:189–205. [PubMed: 18052110]
15. Gay SC, Zhang H, Wilderman PR, Roberts AG, Liu T, Li S, Lin HL, Zhang Q, Woods VL Jr. Stout CD, Hollenberg PF, Halpert JR. Structural analysis of mammalian cytochrome P450 2B4 covalently bound to the mechanism-based inactivator tert-butylphenylacetylene: Insight into partial enzymatic activity. Biochemistry. 2011; 50:4903–4911. [PubMed: 21510666]
16. Zhang H, Lin HL, Walker VJ, Hamdane D, Hollenberg PF. Tert-butylphenylacetylene is a potent mechanism-based inactivator of cytochrome P450 2B4: Inhibition of cytochrome P450 catalysis by steric hindrance. Mol. Pharmacol. 2009; 76:1011–1018. [PubMed: 19720728]
17. Kenaan C, Zhang H, Hollenberg PF. A quantitative high-throughput 96-well plate fluorescence assay for mechanism-based inactivators of cytochromes P450 exemplified using CYP2B6. Nat Protoc. 2010; 5:1652–1658. [PubMed: 20885377]
18. Kuby, SA. Enzyme Catalysis, Kinetics, and Substrate Binding. Vol. Vol. I. CRC Press; Boca Raton, FL: 1991. A study of enzymes.
19. Kent UM, Bend JR, Chamberlin BA, Gage DA, Hollenberg PF. Mechanism-based inactivation of cytochrome P450 2B1 by n-benzyl-1-aminobenzotriazole. Chem Res Toxicol. 1997; 10:600–608. [PubMed: 9168259]
20. Zhang H, Kenaan C, Hamdane D, Hoa GH, Hollenberg PF. Effect of conformational dynamics on substrate recognition and specificity as probed by the introduction of a de novo disulfide bond into cytochrome P450 2B1. J. Biol. Chem. 2009; 284:25678–25686. [PubMed: 19605359]
21. McCoy AJ, Grosse-Kunstleve RW, Adams PD, Winn MD, Storoni LC, Read RJ. Phaser crystallographic software. J Appl Crystallogr. 2007; 40:658–674. [PubMed: 19461840]
22. Adams PD, Grosse-Kunstleve RW, Hung LW, Ioerger TR, McCoy AJ, Moriarty NW, Read RJ, Sacchettini JC, Sauter NK, Terwilliger TC. Phenix: Building new software for automated crystallographic structure determination. Acta Crystallogr Sect D Biol Crystallogr. 2002; D58:1948–1954. [PubMed: 12393927]
23. Emsley P, Lohkamp B, Scott W, Cowtan K. Features and development of coot. Acta Crystallogr Sect D Biol Crystallogr. 2010; D66:486–501. [PubMed: 20383002]
24. Lebedev AA, Young P, Isupov MN, Moroz OV, Vagin AA, Murshudov GN. Jligand: A graphical tool for the CCP4 template-restraint library. Acta crystallogr Sect D Biol crystallogr. 2012; 68:431–440. [PubMed: 22505263]
25. Paul KG, Theorell H, Akeson A. The molar light absorption of pyridine ferroprotoporphyrin (pyridine hemochromogen). Acta Chem. Scand. 1953; 7:1284–1287.

26. Morris GM, Goodsell DS, Huey R, Olson AJ. Distributed automated docking of flexible ligands to proteins: Parallel applications of Autodock 2.4. J Comput Aided Mol Des. 1996; 10:293–304. [PubMed: 8877701]
27. Case DA, Cheatham TE 3rd, Darden T, Gohlke H, Luo R, Merz KM Jr. Onufriev A, Simmerling C, Wang B, Woods RJ. The Amber biomolecular simulation programs. J. Comput. Chem. 2005; 26:1668–1688. [PubMed: 16200636]
28. Park JY, Harris D. Construction and assessment of models of CYP2E1: Predictions of metabolism from docking, molecular dynamics, and density functional theoretical calculations. J. Med. Chem. 2003; 46:1645–1660. [PubMed: 12699383]
29. Harlow GR, Halpert JR. Analysis of human cytochrome P450 3A4 cooperativity: Construction and characterization of a site-directed mutant that displays hyperbolic steroid hydroxylation kinetics. Proc Natl Acad Sci U S A. 1998; 95:6636–6641. [PubMed: 9618464]
30. Hartman JH, Boysen G, Miller GP. CYP2E1 metabolism of styrene involves allostery. Drug Metab dispos. 2012; 40:1976–1983. [PubMed: 22807108]
31. Sohl CD, Isin EM, Eoff RL, Marsch GA, Stec DF, Guengerich FP. Cooperativity in oxidation reactions catalyzed by cytochrome P450 1A2: Highly cooperative pyrene hydroxylation and multiphasic kinetics of ligand binding. J. Biol. Chem. 2008; 283:7293–7308. [PubMed: 18187423]
32. Lin HL, Zhang H, Noon KR, Hollenberg PF. Mechanism-based inactivation of CYP2B1 and its F-helix mutant by two tert-butyl acetylenic compounds: Covalent modification of prosthetic heme versus apoprotein. J. Pharmacol. Exp. Ther. 2009; 331:392–403. [PubMed: 19700628]
33. Kent UM, Mills DE, Rajnarayanan RV, Alworth WL, Hollenberg PF. Effect of 17α-ethynylestradiol on activities of cytochrome P450 2B (P450 2B) enzymes: Characterization of inactivation of P450s 2B1 and 2B6 and identification of metabolites. J Pharmacol Exp Ther. 2002; 300:549–558. [PubMed: 11805216]
34. Silverman RB. Mechanism-based enzyme inactivators. Methods Enzymol. 1995; 249:240–283. [PubMed: 7791614]
35. Davis IW, Murray LW, Richardson JS, Richardson DC. Molprobity: Structure validation and all-atom contact analysis for nucleic acids and their complexes. Nucleic Acids Res. 2004; 32:W615–619. [PubMed: 15215462]
36. Scott EE, White MA, He YA, Johnson EF, Stout CD, Halpert JR. Structure of mammalian cytochrome P450 2B4 complexed with 4-(4-chlorophenyl)imidazole at 1.9-Å resolution: Insight into the range of P450 conformations and the coordination of redox partner binding. J. Biol. Chem. 2004; 279:27294–27301. [PubMed: 15100217]
37. Bridges A, Gruenke L, Chang YT, Vakser IA, Loew G, Waskell L. Identification of the binding site on cytochrome P450 2B4 for cytochrome *b5* and cytochrome P450 reductase. J Biol Chem. 1998; 273:17036–17049. [PubMed: 9642268]
38. Mak PJ, Zhang H, Hollenberg PF, Kincaid JR. Defining the structural consequences of mechanism-based inactivation of mammalian cytochrome P450 2B4 using resonance raman spectroscopy. J. Am. Chem. Soc. 2010; 132:1494–1495. [PubMed: 20078059]
39. Zhang H, Lin HL, Kenaan C, Hollenberg PF. Targeting of the highly conserved threonine 302 residue of cytochromes P450 2B family during mechanism-based inactivation by aryl acetylenes. Arch. Biochem. Biophys. 2011; 507:135–143. [PubMed: 20836985]
40. Lin HL, Zhang H, Waskell L, Hollenberg PF. Threonine-205 in the F helix of P450 2B1 contributes to androgen 16β-hydroxylation activity and mechanism-based inactivation. J. Pharmacol. Exp. Ther. 2003; 306:744–751. [PubMed: 12721329]
41. Shahrokh K, Cheatham TE 3rd, Yost GS. Conformational dynamics of CYP3A4 demonstrate the important role of Arg212 coupled with the opening of ingress, egress and solvent channels to dehydrogenation of 4-hydroxy-tamoxifen. Biochim Biophys Acta. 2012; 1820:1605–1617. [PubMed: 22677141]
42. Oezguen N, Kumar S, Hindupur A, Braun W, Muralidhara BK, Halpert JR. Identification and analysis of conserved sequence motifs in cytochrome P450 family 2. Functional and structural role of a motif ^{187}RFDYKD^{192} in CYP2B enzymes. J. Biol. Chem. 2008; 283:21808–21816. [PubMed: 18495666]

43. Harlow GR, Halpert JR. Alanine-scanning mutagenesis of a putative substrate recognition site in human cytochrome P450 3A4. Role of residues 210 and 211 in flavonoid activation and substrate specificity. J Biol Chem. 1997; 272:5396–5402. [PubMed: 9038138]

44. He Y, Luo Z, Klekotka PA, Burnett VL, Halpert JR. Structural determinants of cytochrome P450 2B1 specificity: Evidence for five substrate recognition sites. Biochemistry. 1994; 33:4419–4424. [PubMed: 8155660]

45. He YA, Balfour CA, Kedzie KM, Halpert JR. Role of residue 478 as a determinant of the substrate specificity of cytochrome P450 2B1. Biochemistry. 1992; 31:9220–9226. [PubMed: 1390709]

46. Zhang H, Amunugama H, Ney S, Cooper N, Hollenberg PF. Mechanism-based inactivation of human cytochrome P450 2B6 by clopidogrel: Involvement of both covalent modification of cysteinyl residue 475 and loss of heme. Mol. Pharmacol. 2011; 80:839–847. [PubMed: 21862689]

47. Scott EE, He YA, Wester MR, White MA, Chin CC, Halpert JR, Johnson EF, Stout CD. An open conformation of mammalian cytochrome P450 2B4 at 1.6-Å resolution. Proc Natl Acad Sci U S A. 2003; 100:13196–13201. [PubMed: 14563924]

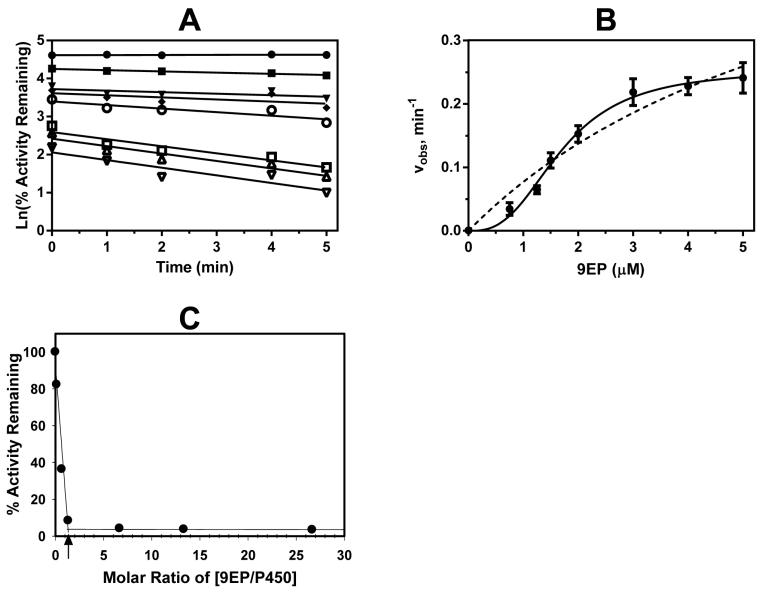

Figure 1.

Characterization of the mechanism-based inactivation of CYP2B4 by 9EP. (A) Time- and concentration-dependent decrease in 7-EFC *O*-deethylase activity. CYP2B4 (0.5 μM) was inactivated at 30 °C in the primary reaction in 50 mM KPi buffer (pH 7.4) containing 1 μM P450 reductase, 1 μM cyt *b5*, and various concentrations of 9EP (0-5 μM), as described in Experimental Procedures. (B) Dependence of the inactivation velocity on the concentrations of 9EP. The velocities were obtained from the data shown in Panel A. The dashed and solid lines are fits to Michaelis-Menten and sigmoidal models respectively. (C) Partition ratio for the mechanism-based inactivation of CYP2B4 by 9EP. The partition ratio was determined in 50 mM KPi (pH 7.4) at various ratios of 9EP to CYP2B4 as described in Experimental Procedures. The solid lines are linear regressions of the activities remaining for the determination of the partition ratio. The arrow indicates the intercept of these two lines with the x-axis.

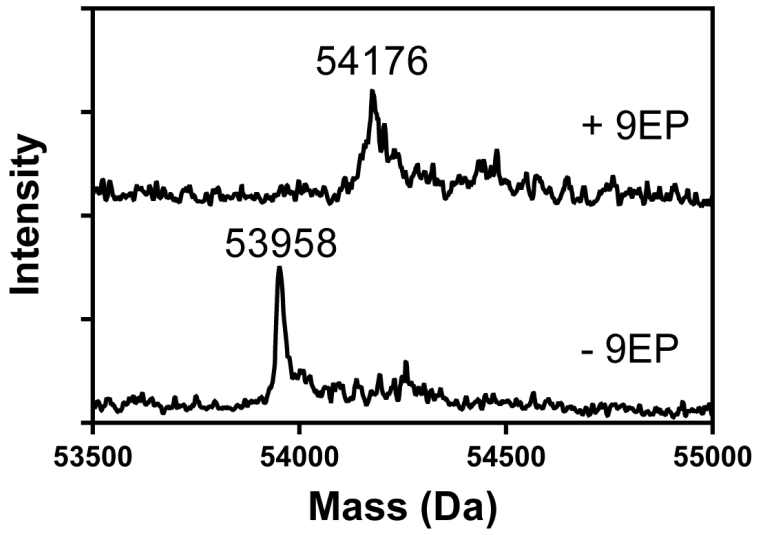

Figure 2.

Analysis of the molecular mass of the 9EP-inactivated CYP2B4 using ESI-LC/MS. CYP2B4 (1 μM) was inactivated by 10 μM 9EP in 50 mM KPi buffer (pH 7.4) in the presence of 0.5 μM CPR, 3 μM cyt *b5* and 1 mM NADPH at 30 °C for 5 min. An aliquot (50 μl) of the reaction mixture was analyzed by LC-MS to determine the molecular mass as described in Experimental Procedures.

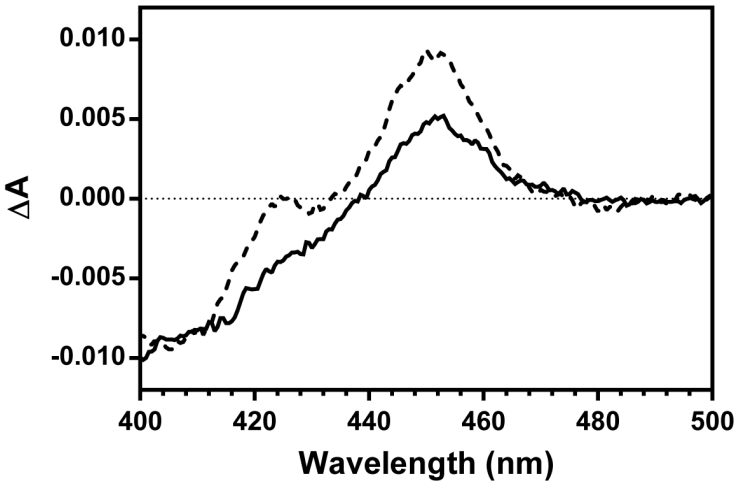

Figure 3.

Loss of the CO-detectable heme during the inactivation of CYP2B4 by 9EP. CYP2B4 (0.2 μM) was inactivated in the presence of 0.6 μM CPR and 10 μM 9EP for 10 min at 30 °C, and the CO difference spectrum was then recorded after the addition of dithionite to the reaction mixture to completely reduce CYP2B4, as described in Experimental Procedures. The control sample was identical to the inactivated sample except that NADPH was absent. The solid and dashed lines represent the CO difference spectra for the inactivated and control samples respectively.

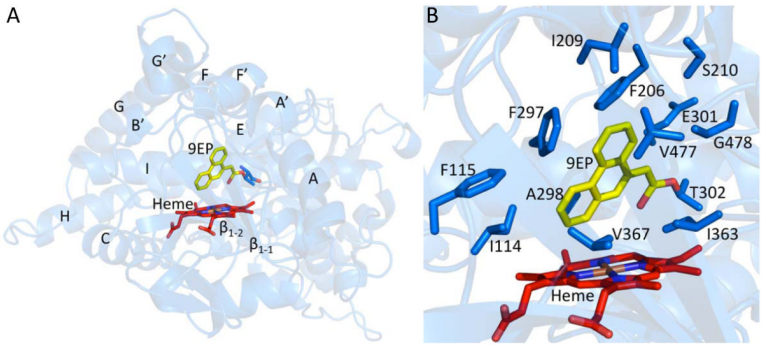

Figure 4.

Crystal structure of the 9EP-modified CYP2B4 showing the overall fold (A) and the architecture of the active site (B). (A) The backbone of the 9EP-modified CYP2B4 is shown as blue ribbons, while the heme and 9EP moiety are shown in red and yellow sticks, respectively. Key α-helices and β-sheets are labeled with either capital letters or Greek letters, respectively. (B) Residues within a radius of 5 Å of the 9EP moiety are shown in blue sticks. The 9EP moiety covalently attached to Thr 302 is colored as yellow stick and the heme is colored as red sticks.

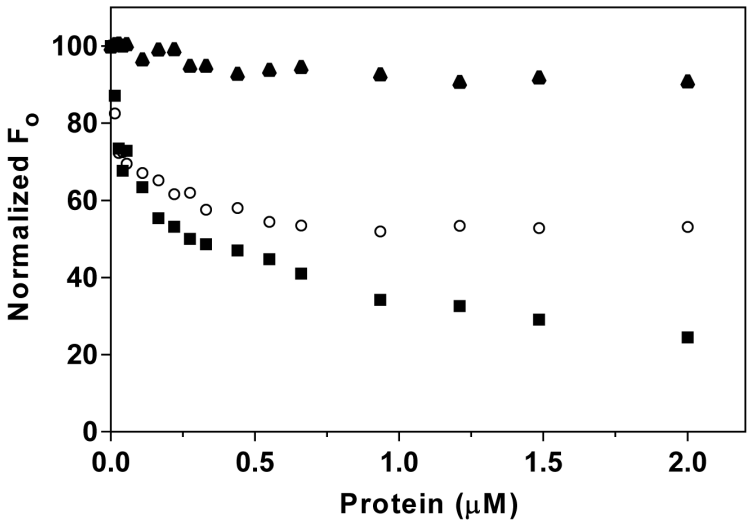

Figure 5.

Quenching of the fluorescence of 9EP upon binding to CYP2B4. Fluorescence emission from 0.5 μM 9EP was quenched by titration with increasing concentrations of unmodified and 9EP-modified CYP2B4 as described in Experimental Procedures. (▲) fluorescence quenching by cyt *c* as negative control; (○) fluorescence quenching by 9EP-modified CYP2B4; (■) fluorescence quenching by unmodified CYP2B4.

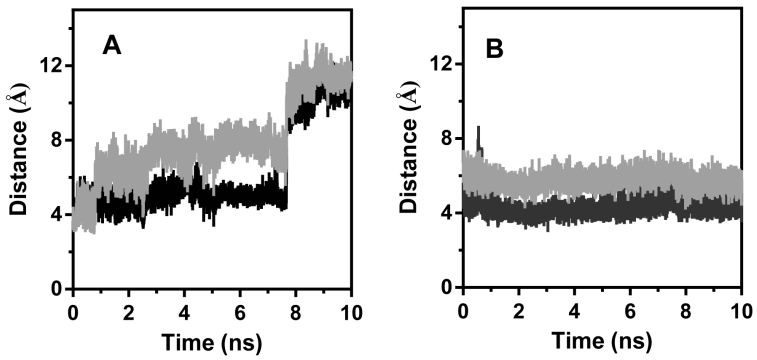

Figure 6.

Analyses of the distances from the terminal carbon (C16) of the acetylene of 9EP to the heme iron (Fe) and the Oγ atom (OG1) of Thr302 in both the binary complex CYP2B4-9EP (A) and the tertiary complex CYP2B4-9EP[2] (B). A 10 ns MD simulation was carried out in explicit water, and the trajectories were analyzed using the ptraj program as described in Experimental Procedures. The dark lines represent the Fe-C16 distances while the grey lines represent the C16-OG1 distances.

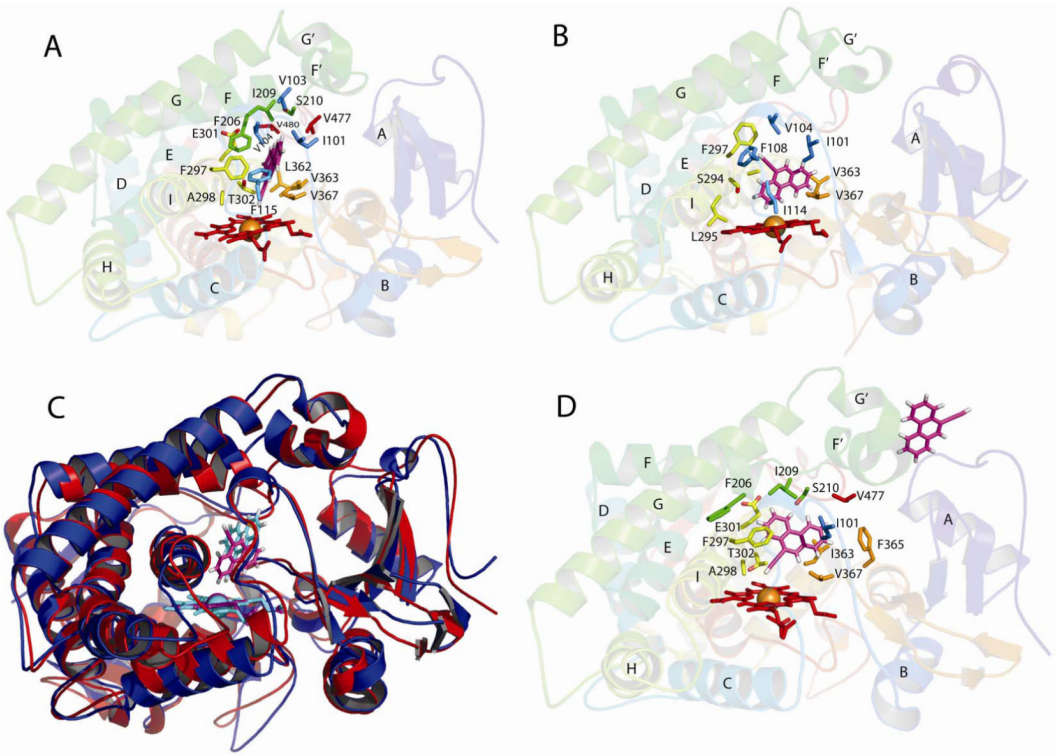

Figure 7.

Snapshots of the secondary structures of the binary and tertiary complexes of CYP2B4 and 9EP. The snapshots were obtained from the MD simulations as described in Experimental Procedures. (A) The starting structure of the CYP2B4-9EP complex prior to unrestricted MD production. The secondary structure is depicted as ribbons colored as rainbow from blue (N-terminus) to red (C-terminus). Residues within 5 Å of the 9EP are shown in sticks, and the heme iron is shown as orange sphere. Key helices are labeled with capital letters. (B) Snapshot at 8.2 ns following the conformational transition of the 9EP in the CYP2B4-9EP complex. Colors and labels are identical to those in Panel A. (C) Superimposition of the two structures shown in Panel A and B based on the alignments of the backbone Cα carbons. The backbone of the starting structure and the one obtained at 8.2 ns are shown in red and blue ribbons respectively. (D) Snapshot at 8.2 ns for the tertiary complex of CYP2B4-9EP[2]. Colors and labels are identical to those in Panel A.

TABLE 1

Data collection and refinement statistics: Values for the highest resolution shell are shown in parentheses

Cytochrome P450	2B4
Crystal Space group	$P3_121$
a = b	90.155 Å
c	148.623 Å
$\alpha = \beta$	90 °
γ	120 °
Molecules per asymmetric unit	1
Wavelength (Å)	1.54
Resolution range (Å)	78.0 - 2.94
Completeness (%)	99.8 (92.6)
Redundancy	7.40 (3.61)
R_{merge} (%)	12.8 (39.5)
I/σ	12.7 (2.1)
No. of unique reflections	15,444
R-factor	24.5 %
R-free	29.6 %
RMS deviations	
Bond lengths (Å)	0.006
Bond angles (°)	0.952
No. of atoms. Average *B*-values (A^2) are in brackets	
Protein	3696 [32.5]
Heme	43 [22.9]
9EP	17 [24.2]
Waters	72 [23.2]
Detergent	34 [69.1]
Tris	22 [61.6]
Molprobity - Ramachandran Plot	
Preferred (%)	97.8
Allowed (%)	2.2

Table 2

Summary of the results obtained from computer-aided docking of 9EP to CYP2B4. The flexible ligand 9EP was docked to the rigid receptor CYP2B4 using Autodock 4.0 as described in Experimental Procedures

Cluster ID	Poses	Binding Energy (kcal/mol)	Locations
1	21	−8.80	Active site
2	45	−7.40	FG loop, A Helix and β1/β2
3	2	−7.30	Between F and G helices
4	4	−7.29	C-terminal side of I Helix
5	14	−7.15	Proximal side of the heme
6	12	−7.13	K Helix and β4 loop
7	2	−7.09	BC loop, β1/β2, and FG loop